

## Reactions of Pyrene Excited States with Oxygen on the Surface of Porous Silica Gel and Similar Surfaces

S. A. Ruetten and J. K. Thomas\*

*Department of Chemistry and Biochemistry, University of Notre Dame, Notre Dame, Indiana 46556*

*Received: August 6, 1998; In Final Form: November 6, 1998*

Oxygen quenching of the singlet state of pyrene adsorbed on amorphous silica gel is studied by pulsed laser and rapid spectrophotometric methods. The quenching rate constant depends on the pore size of the silica and the method and temperature used to remove adsorbed water and surface silanol groups. The two possible mechanisms for O<sub>2</sub> quenching of excited pyrene on an SiO<sub>2</sub> surface are quenching by direct collision encounter on the excited state (Eley–Rideal) and quenching by surface adsorbed oxygen (Langmuir–Hinshelwood). In the present system, these two mechanisms are distinguished using temperature studies. Both mechanisms are operative in the current system: the Eley–Rideal mechanism dominates at temperatures greater than 30 °C, and the Langmuir–Hinshelwood mechanism dominates at lower temperatures,  $T < 10$  °C. Several other surfaces are also briefly studied in order to add insight into the surface processes which are involved. One product of the oxygen quenching of the singlet excited state is the triplet state. Quenching of the singlet state leads to an increase in the triplet yield for pyrene and coronene. However, the efficiency of the oxygen-induced intersystem crossing is much smaller on the SiO<sub>2</sub> surface compared to that in solution. The pyrene triplet excited state is also quenched by oxygen. Unlike the singlet state, the quenching mechanism is predominantly Eley–Rideal or direct collision of oxygen with the excited triplet state on the surface. The efficiency of the triplet quenching decreases with increasing oxygen pressure. This is explained by the formation of an intermediate O<sub>2</sub>–triplet state complex.

### Introduction

The photoreactions of arenes adsorbed on SiO<sub>2</sub> are of current and keen interest, and it is pertinent to inquire about the effect of surface OH content on these reactions. A simple reaction of photochemical interest is the quenching of an arene excited state located on the surface by oxygen contained in the gas space above the solid. Quenching may occur by direct O<sub>2</sub> collision encounter of the excited state, the Eley–Rideal (ER)<sup>1a</sup> mechanism, or by diffusion of surface adsorbed oxygen to the reactive center, the Langmuir–Hinshelwood (LH)<sup>1b</sup> mechanism. Early work<sup>2a</sup> studying the quenching of triplet excited benzophenone on SiO<sub>2</sub> suggested that O<sub>2</sub> quenching occurred by direct collision encounter of the excited state. Later work<sup>2b</sup> studying the O<sub>2</sub> quenching of zinc tetraphenylporphyrin on SiO<sub>2</sub> viewed the process as one whereby oxygen was adsorbed to the surface at the moment of quenching. Further studies on the O<sub>2</sub> quenching of singlet excited pyrene on SiO<sub>2</sub><sup>3a,b</sup> and on alumina<sup>3c</sup> also supported a role for adsorbed O<sub>2</sub> in the quenching process. Other studies<sup>4</sup> have used immobilized ruthenium trisbipyridine to study the oxygen quenching process on surfaces. It is important to investigate the roles played by both the LH and ER mechanisms on the quenching of excited states of arenes adsorbed on SiO<sub>2</sub>.

Silica gel is viewed as an amorphous, porous, large surface-area solid, where the surface of the material is covered with silanol groups to the extent of 5 OH/nm<sup>2</sup>.<sup>5</sup> The OH groups may be geminal or located on the same Si atom, vicinal or located on adjacent Si atoms, or isolated on the surface. Infrared data indicate that all three different OH types may exist on the same material, while the amorphous nature of the solid suggests that

a distribution of these various types of OH exists. Some areas will contain a higher average OH content at the expense of more sparsely populated areas. Narrow regions of pore space or cracks may also occur. It is concluded that arenes are physisorbed to the surface OH groups.<sup>6</sup> The heating process condenses OH groups in close proximity to produce siloxane bridges and H<sub>2</sub>O. It is reasonable to suggest that the areas of high OH content disappear first, and this is supported by IR studies.<sup>5</sup> Studies have shown a reduction in the arene adsorption after the surface OH content is reduced by heating the SiO<sub>2</sub> at high temperatures.<sup>6</sup>

This work uses the effect of temperature and different surface conditions to elucidate the role played by both the LH and ER processes over a wide temperature range. Thermal pretreatment gives rise to surface modifications suggesting changes in surface features can influence each process. Other surfaces are studied and some results are included for comparison to support the conclusions made for the SiO<sub>2</sub> surface.

### Experimental

Steady-state absorption spectra were obtained for liquid and solid samples with a UV–vis Varian Cary-3 spectrophotometer. The instrument is equipped with a diffuse reflectance integrating sphere attachment for the measurement of solid samples. Uncorrected reflectance spectra of powder samples were recorded against PTFE or MgO standards. Samples were placed in 3 mm thick quartz cells with front face powder exposure dimensions of 10 mm wide by 30 mm tall. Identical quartz cells were used in the reference and sample sides of the integrating sphere. The same PTFE holders were used with solution samples, and MgO or PTFE disks were used in the reference channel.

\* Author to whom correspondence should be addressed.

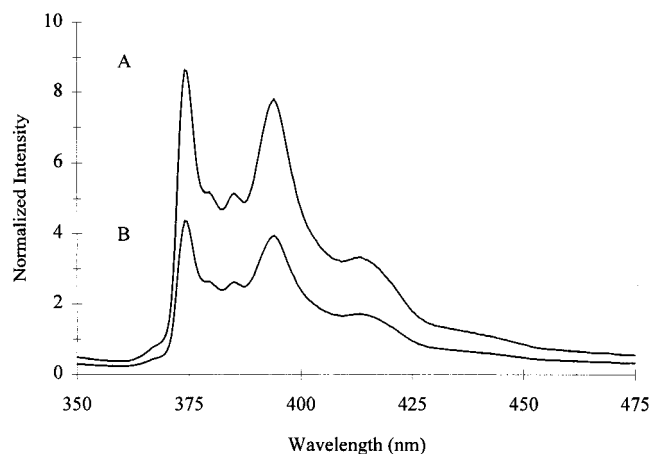


**Figure 1.** Emission spectra for pyrene on silica gel. Emission spectra are shown in vacuum (A) and with 0.5 torr of added oxygen (B). Excitation was at 337 nm for 0.5  $\mu\text{mol/g}$  pyrene on 60 Å silica pretreated at 150 °C in air.

Fluorescence spectra were obtained using a SLM/Aminco SPF-500C spectrofluorometer. The instrument is equipped with a LX300 Xe lamp and a Hamamatsu R-928P photomultiplier. The spectrofluorometer was used for emission spectra, excitation spectra, and time-dependent analysis at a fixed emission wavelength. Emission of the fluorophore was collected at 90° incident to the excitation source. The excitation light was passed through a neutral density filter to minimize sample decomposition. After collection, data from the fluorescence instrument were stored on an IBM-compatible computer. The typical band-pass for routine emission spectra was 7.5 nm for the excitation channel and 1 nm for the emission channel. For the excitation spectra, the band-pass was 7.5 nm for the emission channel and 2 nm for the excitation channel.

The emission spectra without and with added oxygen are shown in Figure 1. The characteristic bands from pyrene are observed in these spectra. The ratio of the third to first bands has been shown to reflect on the environment of this surface probe.<sup>6</sup> Pyrene is located in a polar environment on silica gel as indicated by the III/I ratio of 0.6 both without and with added oxygen.

Fluorescence decays were obtained by excitation of the fluorophore with a 337.1 nm PRA Nitromite nitrogen laser model LN-100 with 0.2 ns fwhm and 70  $\mu\text{J}$  pulse. Additionally, a model LN-1000 PRA nitrogen laser with a 337.1 nm pulse of 1.2 ns fwhm and 1.4  $\mu\text{J}$ , or a Laser-Photonics model UV-24 nitrogen laser with a 337.1 nm pulse of 4 ns and 3 mJ pulse, was used. The laser pulse illuminated the sample at 90° relative to the collection optics. The emitted light was collected through a lens system and detected by a Hamamatsu R-1644 micro-channel plate having a cumulative response time of 0.2 ns. A Bausch and Lomb monochromator (1350 lines/mm, blazed at 400 nm) was used for the selection of the monitoring wavelength. The emitted light was passed through various cutoff and band-pass filters to remove scattered light. The analog signal from the PMT was transferred to an IBM-compatible computer through a 750 MHz programmable waveform digitizer (Tektronix 7912HB, 7A13 differential amplifier) for processing.

Analyzing light for the transient absorption studies was obtained from a 450 W Oriel Xe arc lamp powered by a model 302 PRA power supply. A model M-305 PRA pulser or in-house pulser was used to increase the intensity of the analyzing light. White light was passed through a UV cutoff filter (KOPP glass #3-74) to eliminate wavelengths below 400 nm and avoid

bleaching of the arene ground state. Translucent samples were excited at 90° relative to the analysis light and sample cell. Diffuse reflected light from opaque samples was collected using a quartz optical fiber that transported the filtered light from the irradiation zone to the entry aperture of the monochromator. A master triggering unit was used to control the timing sequence prior to collection of the transient signal. This apparatus controlled the digitizer and determined the opening of the analysis light shutter, the pulsing of the Xe lamp, the collection of  $I_0$ , and the firing of the laser.

Wavelength selectivity was accomplished using specific cutoff and band-pass filters and a Bausch and Lomb monochromator. The signal output was detected by a Hamamatsu R-928P photomultiplier, and the analog signal was captured using a Tektronix model 7912AD programmable digitizer with a 0.4 ns response time. A typical data collection scheme included a Tektronix 7B10 timebase and 7A13 differential comparator with an IBM-compatible computer system. The transmitted light,  $I_0$ , was captured with an A/D converter (Tektronix 7D12) equipped with a M2 Sample and Hold module. The time-resolved signal was converted to absorption versus time. The system response time was approximately 5 ns.

The diffuse reflectance laser flash photolysis data were reported as  $1 - R_t$  given by eq 1.

$$1 - R_t = (I_0 - I_t)/I_0 \quad (1)$$

$I_0$  is the initial reflected light before laser excitation and  $I_t$  is the reflectance of the sample at time ( $t$ ) following laser excitation. Wilkinson et al.<sup>7</sup> have used this function for time-resolved reflectance studies and found  $1 - R_t$  to be linear with the amount of transient present in powdered samples when  $1 - R_t$  is less than 0.1. This function is applicable where the transient concentration decreases exponentially with penetration depth into the powder.<sup>7</sup>

**Surface Area – Pore Size (BET).** The surface area and pore sizes of the silica gel powders measured by the BET<sup>8</sup> method were used as supplied by the manufacturer. Some samples were checked with a Micromeritics surface area analyzer model ASAP 2400. Adsorption isotherms of nitrogen (77 K) and oxygen (77 K) were measured volumetrically using a glass BET system with a greaseless vacuum system. The values agreed with values found in the literature. The powder samples were outgassed for 2 h at 423 K before use.

**Temperature Regulation.** Sample temperatures were regulated by placing the evacuated sample in a quartz Dewar with a thermocouple attached to the backside of the quartz cell. Temperatures between 300 and 77 K were obtained by blowing cold nitrogen through a copper tube which was immersed in a liquid nitrogen bath and focused on the front face of the sample cell above the level of solid inside the cell. Temperature regulation was achieved by adjusting the depth of the liquid nitrogen bath and the flow rate of the nitrogen through the bath. Room-temperature air was blown across the outer front surface of the quartz Dewar to avoid surface fogging. The temperature of the silica inside the cell was calibrated using two thermocouples/detectors, one thermocouple in the silica inside the cell, and the other thermocouple attached to the backside of the cell during data collection. For the samples inside the quartz Dewar, the difference between the inside and outside of the sample cell is less than 3 K for temperatures between 300 and 80 K.

**Silica Gel Powders.** Commercial porous silica gels, Davisil, were manufactured by the Davison Company, a subsidiary of W. R. Grace, and purchased from Aldrich. The silica was routinely washed with weakly acidic (pH 6.0), column-purified,

doubly distilled water and preheated at the desired temperature ( $T_a$ , activation temperature) before use. Nonporous silica gel Cabosil (HS-5) was obtained from Cabot Corporation. The BET surface area was 325 m<sup>2</sup>/g and the particle diameter was 0.008  $\mu$ m as supplied in the manufacturer's technical data sheets.<sup>9</sup> The 60 Å Davisil silica gel was pretreated by washing in slightly acidic water, distilled water, followed by heating at 150 °C in air. Dehydroxylation of the silica gel was carried out thermally by static heating of the powders either in air or in a vacuum at elevated temperatures.

Pyrene (Aldrich, 99%) in C<sub>6</sub>H<sub>12</sub> was purified by three passes through an activated silica gel column. Bromopyrene from AGFA was recrystallized three times from methanol followed by passing a C<sub>6</sub>H<sub>12</sub> solution over silica gel. HPLC measurements indicated less than a 0.01% pyrene impurity in the bromopyrene. The triplet decay rate for bromopyrene in methanol after purification was 19  $\mu$ s compared to a literature value of 20  $\mu$ s.<sup>10</sup> Before use, coronene and anthracene were recrystallized from ethanol, and the fluorescence decay lifetimes and absorbance spectra matched the literature results.

All other solvents were HPLC grade from Aldrich and were dried over molecular sieve before use. Cyclohexane (99%) was dried with an activated molecular sieve and passed down an activated silica column before use. All solutions were deoxygenated using a flow of solvent saturated nitrogen for 10 to 20 min or until the emission of the pyrene singlet excited state at 392 nm was constant for each solvent.

Prepurified oxygen was used as received from the Mittler Co. Specific amounts of dry oxygen were added from a 1 L reservoir on the vacuum system. The O<sub>2</sub>–SiO<sub>2</sub> samples were allowed to equilibrate for 5 min in a fixed position cell holder before measurements were taken. The equilibration O<sub>2</sub> pressure was recorded before and after exposure to the sample and the amount of any oxygen adsorbed to the sample could be calculated.

The oxygen desorption studies were performed using a fixed sample configuration and by using a large evacuated chamber to rapidly remove the gaseous oxygen in the sample cell. For the oxygen dose response plots, at least seven different randomly applied oxygen pressures were used.

**Sample Preparation.** Fluorophores, such as pyrene, were adsorbed to the silica gel surface from cyclohexane or hexane solutions of these compounds. Standard pretreatment conditions included gently washing the SiO<sub>2</sub> in pH 6.5 water, distilled water, and drying for 24 h at 150 °C in air. A solution of the fluorophore at the desired concentration in dry cyclohexane was added to SiO<sub>2</sub> in a vial and stirred for 30 min in order to reach maximum absorption of the fluorophore on the high-surface-area powder. Further stirring for 2 h total did not significantly increase the amount of fluorophore adsorbed to the SiO<sub>2</sub> sample. An aliquot of the supernatant was checked spectroscopically for percent fluorophore adsorption. Pyrene was added to the 60 Å silica from cyclohexane to give a typical final surface concentration of 0.45  $\mu$ mol/g.

The silica/cyclohexane slurry was transferred to a 0.2 or 0.3 cm thick quartz cell fitted with a stopcock with minimal exposure to ambient atmosphere. The pyrene-loaded dry powder was never exposed to the ambient atmosphere during the preparation. The excess solvent was removed slowly under vacuum at room temperature, typically at least 2 h, and finally evacuated at 100–120 °C for 20 min under vacuum immediately before use. Silica disks prepared under identical conditions showed no increase in the 3700 cm<sup>−1</sup> water band in the infrared

spectra for low (150 °C) or high-activation-temperature silica (600 °C), indicating this procedure did not add water to the sample.

Pyrenebutyric acid (PBA) was recrystallized from methanol and prepared as a concentrated solution in acetone. Following solvent evaporation in a stream of blowing dry nitrogen, dry cyclohexane and silica gel were added and stirred for 2 h following the above procedure for pyrene. Spectroscopic analysis of the PBA-loaded silica and the sample vial indicated that 100% of the added PBA was adsorbed on the silica powder under these conditions.

Pyrene was covalently attached to 60 and 150 Å silica following a modification of the procedure by Creary<sup>11</sup> and Silva et al.<sup>12</sup> using 1-pyrenyldiazomethane. The pyrene intermediate was attached to the surface silanol groups by thermal reaction at 150 °C, which gave a 40% yield. This resulted in a final pyrene loading of 0.45  $\mu$ mol/g as estimated from the absorption spectrum compared to a pyrene standard on silica. The treated surface was washed rigorously with methanol, acetonitrile, and finally cyclohexane.

In solution, the observed rate constant,  $k_{\text{obs}}$ , without added quencher is obtained from the first-order plot of the decay profile and is given by eq 2.

$$I_t = I_o \exp(-k_{\text{obs}} t) \quad (2)$$

A computer fit to the digitized decay profile was made for all decay data using an iterative least-squares optimization computer program. The least-squares iterative fitting procedure minimizes the  $\chi^2$  residual. In more complicated systems, where environmental inhomogeneity changes the deactivation characteristics, a more complex model is required. The decay of the singlet excited state of pyrene on silica gel has been modeled by a Gaussian distribution<sup>3</sup>.

**Water Content of SiO<sub>2</sub>.** The residual water content of the powdered silica was estimated from pressed disks of the low- and high-activated-temperature silica. Pressed disks were added to the pyrene/cyclohexane solutions and evacuated in a manner similar to the powder samples. The surface OH stretching bands and the bands from the surface-adsorbed water were measured before and after doping the self-supporting disks with a known amount of water. The residual water content estimated from the infrared studies for the  $T_a = 150$  °C sample is less than 1.0  $\mu$ mol/g. The high  $T_a$  sample (600 °C) is reported to contain approximately 1 OH/nm<sup>2</sup>.<sup>5</sup> No detectable water was seen on the 600 °C sample heated for 24 h in air. The reproducibility of the water content measurements is about  $\pm 25\%$  and results from the disk-preparation and sample-doping inaccuracies. The results indicate the presence of small to indeterminable amounts of residual water on the pressed disk samples using the above pyrene doping technique. The powder silica samples are expected to contain less residual water, as the dried powder samples are not exposed to ambient conditions of moisture before use. The disks contain residual water adsorbed during the mounting of the disk in the infrared cell. This water is removed by heating the disk at 125 °C in a vacuum for 15 min.

The standard literature for silica gel<sup>5</sup> states that heating SiO<sub>2</sub> to 600 °C removes surface silanol groups while the basic structure remains intact. Our measurements are in agreement with previous reports<sup>5</sup> in that the surface area is unaltered by our treatment over the temperature range used.

## Results

**Time-Resolved Fluorescence Studies.** Figure 2 shows the time-decay profile of the fluorescence of pyrene on SiO<sub>2</sub>, with



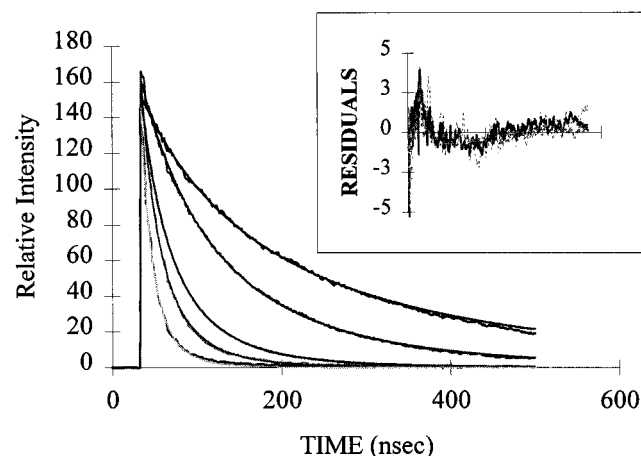


**Figure 2.** Decay profiles of the pyrene singlet excited state at 400 nm after laser excitation at 337 nm shown with increasing concentrations of added oxygen. Pyrene at 0.5  $\mu\text{mol/g}$  on 60 Å silica pretreated at 150 °C in air was used. From top to bottom decay traces represent oxygen pressures of 0, 0.71, 6.2, 11.7, and 34.5 torr. The solid lines are the gaussian fit to the actual data. The inset shows a residual plot for the difference between the actual data and the gaussian fit.

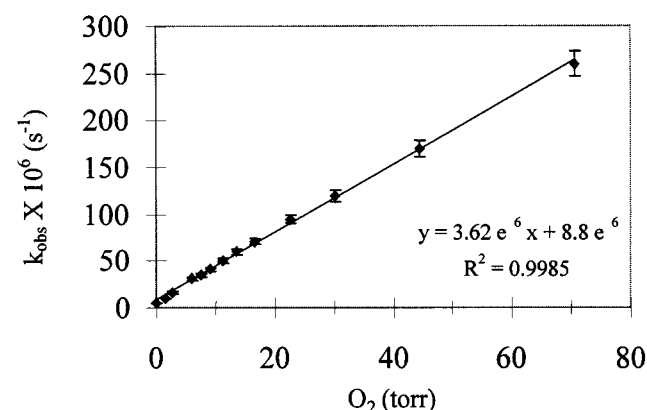


**Figure 3.** Decay rate constants of the pyrene singlet excited state at 400 nm plotted against increasing oxygen concentration. The solid line is the best-fit line to the actual data. The slope of  $3.62 \times 10^6$  is in  $\text{torr}^{-1} \text{s}^{-1}$  as discussed in the text. The 6 % error bars were determined from triplicate measurements of the same oxygen pressures using different measurements of the same sample.

and without addition of oxygen; oxygen increases the rate of decay of the fluorescence. As in earlier work<sup>3</sup> the decay profiles are fitted by a Gaussian function to account for the heterogeneous nature of the various adsorption sites for pyrene. The fits to the actual data are excellent. The decay rates,  $k_{\text{obs}}$ , obtained from the fits are plotted against oxygen pressure in Figure 3. The linearity of the plots lends confidence to the conventional eq 3,

$$k_{\text{obs}} = k_0 + k_q [\text{Q}] \quad (3)$$

where  $k_0$  and  $k_{\text{obs}}$  are the rate constants of the decay in the absence and presence of oxygen, respectively,  $k_q$  is the quenching rate constant, and  $[\text{Q}]$  is the oxygen concentration. Table 1 shows the quenching rate constants obtained from plots such as those in Figure 3. The  $k_q$  is quoted in  $\text{Torr}^{-1} \text{s}^{-1}$  as measured, and also as  $\text{dm}^3 \text{mol}^{-1} \text{s}^{-1}$ , the more common units. The rates for all surfaces, apart from Laponite, lie in the range  $2.8$  to  $8.5 \times 10^6 \text{ Torr}^{-1} \text{s}^{-1}$ . However, differences do exist between the different surfaces. The quenching constants for different probes on these surfaces also exhibit differences and these are given in Table 2. An exact interpretation of these phenomena would

**TABLE 1: Dynamic Quenching Rate Constants for the Pyrene Singlet Excited State by Oxygen on Surfaces at Room Temperature<sup>a</sup>**

surface	S.A. ( $\text{m}^2/\text{g}$ )	$k_q^b$ ( $\text{torr}^{-1} \text{s}^{-1}$ ) $\times 10^6$	$k_q$ ( $\text{dm}^3 \text{mol}^{-1} \text{s}^{-1}$ ) $\times 10^{10}$
M40	680	3.5	6.4
D60	480	3.6	6.49
D150	325	6.6	12.2
Cabosil	325	2.8	5.08
60 Å derivatized	480	8.4	15.4
150 Å derivatized	325	8.3	15.3
SiAl	460	8.5	15.5
Laponite	(310)	1.0	1.83
NaCl <sup>b</sup>	10	4.8	8.6

<sup>a</sup> M40 is 40 Å Merck, D60 is 60 Å Davisil, D150 is 150 Å Davisil, Cabosil is HS-5 nonporous, SiAl is silica alumina (13%  $\text{Al}_2\text{O}_3$ ). All surfaces were pretreated at 150 °C before use and 0.45  $\mu\text{mol/g}$  pyrene was added from cyclohexane; for NaCl 0.1  $\mu\text{mol/g}$  pyrene was used. <sup>b</sup> For all measurements triplicate determinations were made and the one standard deviation for the measurements is  $\pm 0.05 \text{ torr}^{-1} \text{s}^{-1}$ . Derivatized silica was prepared as described in the Experimental section.

**TABLE 2: Singlet Quenching Rate Constants for Probes on Silica Gel and Silica-Alumina with Oxygen at Room Temperature<sup>a</sup>**

probe (surface pretreatment)	$(k_q \text{ in } \text{L mol}^{-1} \text{s}^{-1} \times 10^{10})$			
	D60 (150 °C)	D60 (650 °C)	D150 (150 °C)	SiAl (150 °C)
coronene	4.1	5.5	5.3	7.9
naphthalene	6.6		11.4	
pyrene	6.5	10.2	11.5	15.6
pyrenebutyric acid	13.0	17.3		
fluoranthene	0.57	0.61		0.60

<sup>a</sup> D60 is 60 Å Davisil, D150 is 150 Å Davisil, SiAl is silica alumina. All probes loaded from cyclohexane to give 0.45  $\mu\text{mol/g}$  final surface concentration. Surface pretreatment temperature is noted as described in the Experimental section. Coronene was used at 0.1  $\mu\text{mol/g}$  on all four surfaces. Excitation was at 337 nm except for naphthalene which was excited at 265 nm.

be difficult. However, it is reasonable to suggest that due to the devious nature of the surface, i.e., pockets of high surface area, OH density, cracks, and pores of various size, that probes such as pyrene adsorb differently in each region. It was established earlier<sup>4</sup> that pyrene is adsorbed to  $\text{SiO}_2$  via the surface silanol groups and areas of high OH density will preferentially adsorb arenes compared to less dense areas. It is expected that the OH density is higher in the cracks or small pores compared to an open or flat  $\text{SiO}_2$  surface. This leads to some probes being more exposed to oxygen than others.

In particular, pyrene butyric acid (PBA) possesses a carboxyl group which adsorbs strongly to  $\text{SiO}_2$ . This tends to locate the pyrene chromophore away from the surface and into the gas phase. In addition, the larger bulk of PBA tends to exclude it from smaller regions on the surface, placing it in more open regions of the surface compared to pyrene. Both suggest that the pyrene chromophore of PBA is more accessible to oxygen than pyrene. This model parallels the larger  $k_q$  results observed for PBA on the surface of  $\text{SiO}_2$  compared to that of pyrene.

Heating the  $\text{SiO}_2$  surface to 650 °C removes OH groups with preference being given to regions of high OH density. The probes then tend to adsorb in more open regions of lower OH density on the 650 °C surface that are more accessible to oxygen. Hence, the  $k_q$  values are increased on the 650 °C surface compared to the 150 °C heated surface. Typical data are shown in Table 2 and in Figure 4. All probes show similar behavior apart from fluoranthene which gave a much lower  $k_q$  on  $\text{SiO}_2$  than was obtained for the other surface-bound probes. This

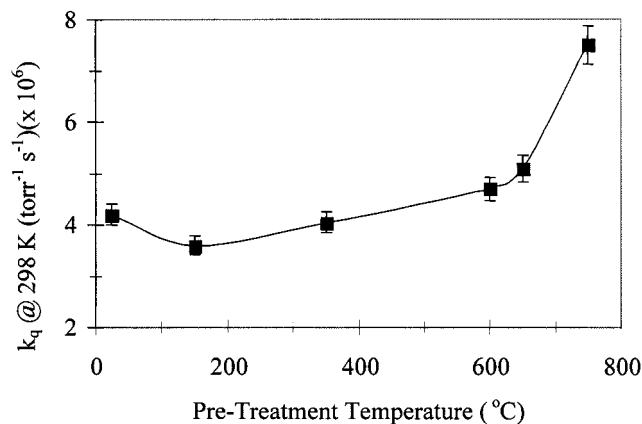


**Figure 4.** The quenching rate constants for 0.45  $\mu\text{mol/g}$  pyrene on 60 Å silica pretreated at different temperatures plotted against the pretreatment temperature. The solid line connects the data points at each temperature. Each point was collected as described in Figures 2 and 3. The silica was washed with water before pyrene adsorption and then dried at the respective temperature for at least 24 hours before pyrene adsorption. The pyrene concentration of the cyclohexane slurry was adjusted for the different adsorption capacity of each surface to give the same final concentration of adsorbed pyrene.

behavior was also observed for fluoranthene in the gas phase relative to other probes and was attributed to a unique arrangement of the triplet energy levels.<sup>13</sup>

It is not pertinent to discuss the SiAl or NaCl surfaces at this time. These data will be discussed later in the text. The clay Laponite has a closely layered structure where chromophores are adsorbed between the layers. Oxygen diffusion is limited in the layered structure<sup>14</sup> leading to smaller quenching rate constants for this system compared to the other surfaces. This is in agreement with the data presented in Table 1.

**Effect of Pyrene Surface Loading.** The  $k_q$  for oxygen increases with increasing pyrene adsorbed on silica gel. Typical data are shown in Figure 5. For both the 60 and 150 Å pore size silicas the oxygen quenching rate constant increases with increasing pyrene loading. This can be interpreted as resulting from changes in the pyrene environment on the surface with pyrene loading; increased pyrene loading causes pyrene adsorption into more open regions on the surface, again increasing the availability of oxygen resulting in increased quenching rate constants.

**Effect of Reaction Temperature.** The  $\text{O}_2$  quenching rate constant,  $k_q$  decreases with decreasing temperature from 148 K reaching a minimum at around 298 K and again increases with the sample temperature up to 410 K. Typical data for the observed quenching by oxygen with  $\text{O}_2$  pressure at various temperatures are shown in Figure 6 for physisorbed pyrene. The linear plots of Figure 6 define the quenching rate constants for each temperature. The quenching rate constants are then plotted against sample temperature in Figure 7a. Covalently bound pyrene shows behavior similar to that of physisorbed pyrene. This figure clearly shows the behavior typical of the two quenching mechanisms discussed earlier. At low temperatures more oxygen is adsorbed on the  $\text{SiO}_2$  surface which enhances the Langmuir–Hinshelwood mechanism. At higher temperatures, oxygen adsorption is decreased which results in a dominant Eley–Rideal mechanism. An analysis of the temperature effect of data from Figure 6 indicates the relative importance of each mechanism.

It is first assumed that oxygen quenching of singlet excited pyrene is not a temperature-activated process, a fact born out later for the gas-phase data.<sup>15</sup> Any temperature effects are

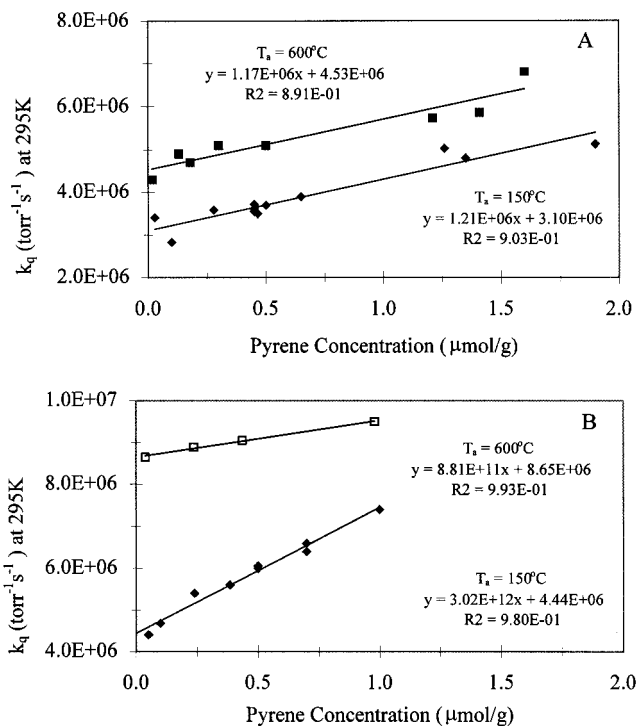


**Figure 5.** The effect of the surface pyrene concentration on the  $\text{O}_2$  quenching of the pyrene fluorescence. (A) The pyrene loading on 60 Å silica gel was increased from 0.02  $\mu\text{mol/g}$  to above 1.5  $\mu\text{mol/g}$  on silica pretreated at 150 and 160 °C. The oxygen quenching rates were collected at room temperature as described in Figures 2 and 3. The oxygen quenching rates for 0.45  $\mu\text{mol/g}$  adsorbed pyrene were collected on seven independently prepared samples made over 18 months. The solid lines are the best-fit regression lines through the actual data. (B) Oxygen quenching rate constants for pyrene on 150 Å silica as in (A). The regression line for the 600 °C pretreated data is calculated from the data between 0.1 and 1.0  $\mu\text{mol/g}$  pyrene.

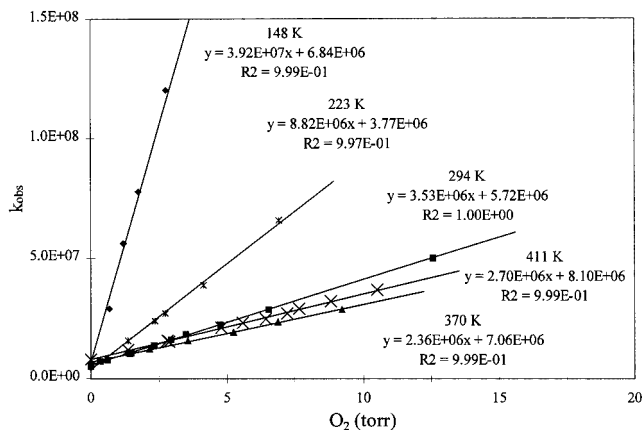


**Figure 6.** Decay rates for the pyrene singlet excited state at 400 nm plotted against the oxygen concentrations for several sample temperatures above and below room temperature. The sample contains 0.45  $\mu\text{mol/g}$  pyrene and the 60 Å silica was pretreated at 150 °C in air before pyrene adsorption. Sample temperatures were controlled as described in the Experimental section of the text.

derived from changes in the rate of collision encounter of the  $\text{SiO}_2$  surface by oxygen, or by increased oxygen adsorption to the surface. The effect of temperature in mechanism I (ER) is given by simple collision theory as,

$$z = n(kT/2\pi m)^{1/2} \quad (4)$$

where  $z$  is the rate of collision of  $\text{O}_2$  with the surface,  $n$  is the

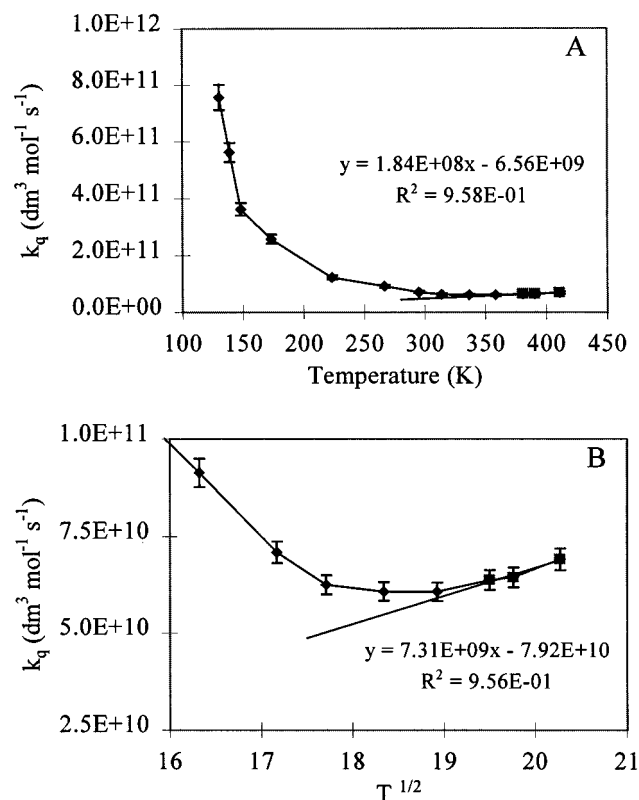


**Figure 7.** (A) The oxygen quenching rate constants for pyrene on 60 Å silica gel are plotted against sample temperature for silica pretreated at 150 °C. The quenching rate constants were calculated from the decay rates at 400 nm as described in the text. (B) The oxygen quenching rate constants are plotted against the square root of temperature between 250 and 411 K. The best-fit regression line is shown as calculated using the highest sample temperature. Two identical samples were used to collect the oxygen quenching rate constants at the highest five temperatures. The error bars show the calculated error from replicate measurements at each temperature and average 5 % CV. Each point on the figure represents the best-fit regression line using a minimum of eight oxygen concentrations for each sample temperature.

oxygen concentration in molecules/cc,  $m$  is the mass of oxygen, and  $k$  and  $T$  are the Boltzman constant and temperature, respectively.<sup>15</sup> This indicates that  $z$ , which is directly proportional to  $k_q$  by the ER mechanism, varies as  $T^{1/2}$ . Such a plot is shown in Figure 7b. The high-temperature end of the plot shows a region of linearity of  $k$  versus  $T^{1/2}$ . Data from higher temperatures is not included as pyrene decomposition on SiO<sub>2</sub> was observed at temperatures above 140 °C. The loss in pyrene emission and the formation of products in the steady-state absorption spectrum clearly showed the thermal decomposition of pyrene at temperatures above 140 °C.

Back extrapolation of the high-temperature data shows that both the ER and LH mechanisms are operative at room temperature. At 20 °C, these mechanisms account for 72 (ER) and 28 (LH) percent, respectively, for O<sub>2</sub> quenching of excited pyrene on 60 Å silica pretreated at 150 °C. Table 3 shows the percentages of the ER mechanism for several SiO<sub>2</sub> surfaces. All pore sizes of SiO<sub>2</sub>, and the Laponite surface show the above temperature-dependent behavior. In contrast, pyrene adsorbed on sodium chloride does not show the same temperature dependence of oxygen quenching.

**Sodium Chloride Surface.** It is pertinent to discuss data that shows that small sodium chloride crystals ( $r = 100$  Å) exhibit only ER behavior over the temperature range used and no O<sub>2</sub> adsorbs on the surface. Typical data are shown in Figure 8. The data for NaCl and SiO<sub>2</sub> surfaces are compared in Figure 9.

**TABLE 3: Predicted Oxygen Quenching from Collision Encounter at Room Temperature and the Percent of the Gas Phase Rate Constant<sup>a</sup>**

surface ( $T_a$ , °C)	measured rate ( $\text{dm}^3 \text{mol}^{-1} \text{s}^{-1}$ ) $\times 10^{10}$	calculated rate ( $\text{dm}^3 \text{mol}^{-1} \text{s}^{-1}$ ) $\times 10^{10}$	%ER	%LH	% of gas phase
NaCl	8.3	8.34	100	0	49
60 Å (150)	6.5	4.65	72	28	27
60 Å (650)	9.5	5.76	61	39	34
Py-SiO <sub>2</sub> (60 Å)	15.8	10.7	68	32	63
150 Å (150)	11.2	8.10	72	28	48

<sup>a</sup> Calculated rates from back extrapolation using the slope and intercept data from plots of  $T^{1/2}$  versus temperature. Rates were calculated at 22 °C using the best-fit lines. %ER and %LH are the percentage of Eley–Rideal and Langmuir–Hinshelwood quenching mechanisms for the measured rate which operates at room temperature as predicted by the temperature data. 0.45 μmol/g pyrene on silica surfaces. 0.1 μmol/g pyrene on sodium chloride.

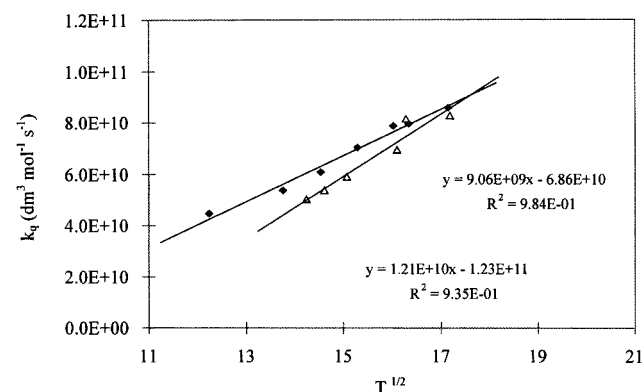


**Figure 8.** The oxygen quenching rate constants plotted against the square root of temperature for pyrene physisorbed on sodium chloride pretreated at 150 °C for 2 h. The two sets of data points and best-fit regression lines are for two independently prepared samples at the same pyrene loadings and pretreatment conditions.

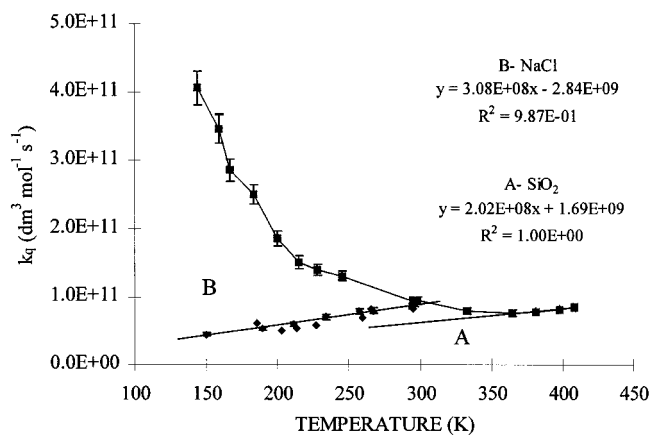


**Figure 9.** The oxygen quenching rate constants for pyrene on silica and sodium chloride plotted against the sample temperature. The regression statistics of the best-fit line using the highest temperature data for pyrene on silica are included with the regression line. The regression line for the pyrene on NaCl sample is calculated using the quenching rate constants at all temperatures for this sample. The data are collected as described in Figure 7 for silica and in Figure 8 for pyrene on sodium chloride.

The linear portions of the curve at the higher temperatures are plots of  $k_q$  versus temperature and give the  $k_q$  due to the ER mechanism. The difference between this predicted value and the total  $k_q$  gives the contribution from the LH mechanism. For SiO<sub>2</sub> the contribution from the LH mechanism is significant at 20 °C; however, as the reaction temperature decreases the LH

contribution to the overall reaction increases. At this stage it is important to comment on the efficiency of the O<sub>2</sub> quenching of excited pyrene.

It is expected that the  $k_q$  for a NaCl surface is entirely due to the ER mechanism. This is supported by the linear dependence of  $k_q$  versus  $T^{1/2}$  for all temperatures tested and by the fact that O<sub>2</sub> does not adsorb to the NaCl surface at the temperatures used. The measured  $k_q$  is 49% of that for pyrene in the gas phase. This can be immediately rationalized by viewing pyrene as being located on a planar NaCl surface, where the approach of O<sub>2</sub> to the surface is limited to 50% of that in the gas phase. A detailed discussion is given later.

## Discussion

**Collision Quenching Rates.** It is possible to comment on the  $k_q$  from the ER mechanism by comparing this rate constant with the corresponding rate constant in the gas phase. The O<sub>2</sub> quenching rate constant of pyrene in the gas phase is reported as  $1.9 \times 10^{11} \text{ L mol}^{-1} \text{ s}^{-1}$  at 115 °C<sup>16,17</sup> and  $2.48 \times 10^{11} \text{ L mol}^{-1} \text{ s}^{-1}$  at 170 °C.<sup>16</sup> The calculated rate constant via collision theory is  $3.06 \times 10^{11} \text{ L mol}^{-1} \text{ s}^{-1}$ .<sup>16</sup> The authors indicate that the probability of quenching is 63% of the calculated rate at 115 °C and 77% at 170 °C. The activation energy is small and to a first approximation the  $T^{1/2}$  dependence of  $k$  on  $T$  is used to calculate  $k_q$  at room temperature. For the gas-phase reaction  $k_q$  is calculated as  $1.66 \times 10^{11} \text{ M}^{-1} \text{ s}^{-1}$  at 298 K.

Table 3 contains the measured  $k_q$  for quenching which is the sum of the ER and LH mechanisms. The contributions of both the ER and LH mechanisms to the  $k_q$  can be calculated as indicated above and are given in Table 3. The rate of the ER process on the surface can be compared to that in the gas phase. In all cases the surface rate constant is smaller than that in the gas phase, due to shielding, as discussed for the NaCl surface. Probes adsorbed on the surface must rely on direct collision encounter and diffusion of oxygen or the diffusion of the probe. The diffusion of pyrene on the SiO<sub>2</sub> surface is negligible<sup>4a</sup> and the rate is then dependent on the diffusion of oxygen.

The quenching rate constant for probes on the surface is reduced compared to the gas phase by the immobilization of pyrene on the surface, and by 50% due to the blocking of the O<sub>2</sub> approach to pyrene on the surface. The rate in the gas-phase  $k_g$  compared to that on the surface  $k_s$  is

$$k_s = \frac{1}{2} \left( \frac{(D_{O_2} + D_p)_s}{(D_{O_2} + D_p)_g} \right) k_g \quad (5)$$

where the  $D$  refers to diffusion constants of the reactants in the gas phase and solid phase. In the solid–gas-phase reactions,  $D_{O_2} \gg D_p$  as pyrene is immobilized at the surface while O<sub>2</sub> is in the gas phase. Hence, eq 5 becomes

$$k_s = \frac{1}{2} \left( \frac{1}{1 + (D_p/D_{O_2})_g} \right) k_g \quad (6)$$

The diffusion constant  $D$  varies as the inverse square root of the molecular weight. Hence,  $(D_p/D_{O_2})$  is 0.3 and then

$$k_s = 0.5 \left( \frac{1}{1.3} \right) k_g \quad (7)$$

indicating the  $k_s/k_g$  is very close to 0.4.

In agreement with this picture, Table 3 shows that the O<sub>2</sub> quenching of pyrene on the SiO<sub>2</sub> surface is much less compared to the gas phase. Surfaces with low surface curvature, e.g., NaCl and 150 Å silica give  $k_s/k_g$  of 0.49 and 0.48, respectively, in

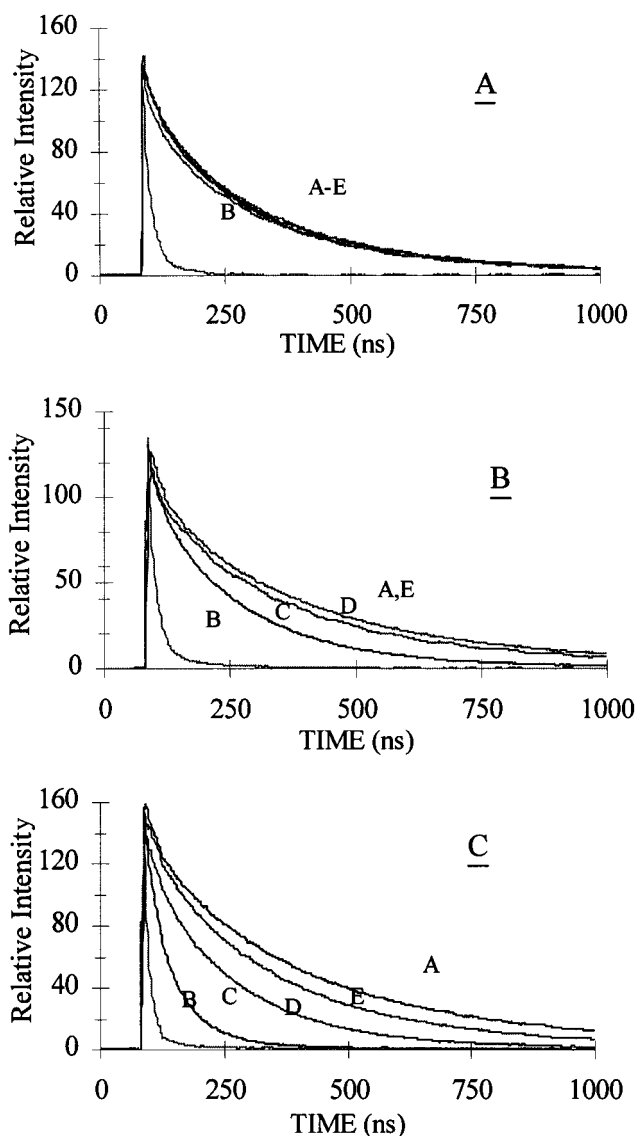


**Figure 10.** The decay profiles for the pyrene excited state at 400 nm are shown for oxygen desorption from 60 Å silica at different sample temperatures. In each panel the unquenched decay profile is shown as the highest profile in the panel. Each panel also shows the decay profile for the sample with 10 torr added oxygen with the vacuum closed as the decay profile with the lowest intensity in the panel. Additional decay profiles between the unquenched and oxygen-quenched profiles represent increasing times of sample evacuation. The sample temperatures are 296 K (Panel A), 183 K (Panel B), and 150 K (Panel C). The decay profiles in panel C from top to bottom are for no oxygen (A), 90 (E), 30 (D), 10 (C), and 0 (B) s of sample evacuation. Similar results are obtained with 4 torr added oxygen.

close agreement with the above picture. The 60 Å silica gives lower values of 0.27 to 0.34 which reflects on the further surface shielding of pyrene from O<sub>2</sub>. The pyrene-derivatized silica acts to place pyrene in a more open position, where it is more accessible to O<sub>2</sub>, increasing the  $k_s/k_g$  ratio.

**Desorption of O<sub>2</sub> from the Surface.** The LH mechanisms require that O<sub>2</sub> is adsorbed on the SiO<sub>2</sub> surface for a short period of time during which it can move to excited pyrene, thus quenching the excited state. This is visualized as a dynamic process where O<sub>2</sub> collides with the surface, leading to an equilibrium of O<sub>2</sub> adsorbed to the surface and O<sub>2</sub> in the gas phase. For SiO<sub>2</sub>, it should be possible to observe this process directly at sufficiently low temperatures. This effect should not be observed for a NaCl surface as O<sub>2</sub> adsorption does not occur on this surface.



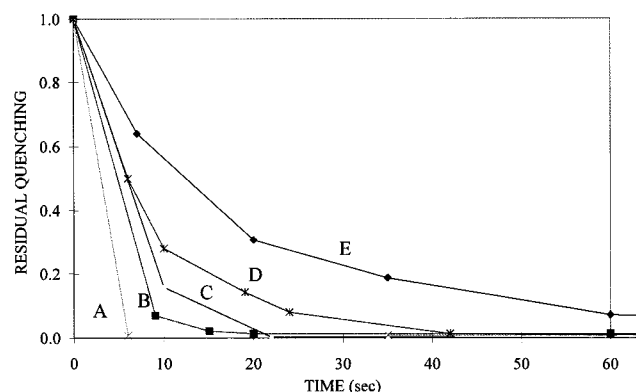


**Figure 11.** The residual quenching of the singlet excited-state lifetimes of pyrene is shown after sample evacuation for increasing times relative to the unquenched lifetime. The decay profiles are shown in Figure 10. 337 nm laser excitation was used. The sample temperatures in the figure are 295 K (A), 250 K (B), 228 K (C), 170 K (D), and 133 K (E).

Oxygen removal from a SiO<sub>2</sub> surface was monitored by steady-state and time-resolved quenching of the pyrene fluorescence. Typical data are shown in Figure 10. The decay profiles of the pyrene fluorescence using 60 Å silica are shown in the presence of O<sub>2</sub> after various periods of O<sub>2</sub> removal by rapid oxygen evacuation. In panel A of Figure 9 a reaction temperature of 296 K is shown with added O<sub>2</sub> which markedly quenches the pyrene fluorescence. However, removal of O<sub>2</sub> immediately (<5 s) restores the system to the original O<sub>2</sub>-free pyrene fluorescence decay condition. As the temperature is lowered, panels B (183 K) and C (150 K), the removal of O<sub>2</sub> becomes slower and measurable on the time scale of seconds. The data from Figure 10 are transformed to Figure 11 which shows the efficiency of quenching at several temperatures and for several time intervals after O<sub>2</sub> removal from the gas phase. For the NaCl surface, at the lowest temperature used, 150 K, pumping the NaCl-pyrene-O<sub>2</sub> system immediately (<5 s) removed the O<sub>2</sub> and the pyrene excited state was no longer quenched. For the SiO<sub>2</sub> system, significantly different results were obtained as the oxygen was slowly removed from the surface. The data for NaCl and SiO<sub>2</sub> clearly supported the ER and LH mechanisms suggested for O<sub>2</sub> quenching of excited states on surfaces.

**Triplet Quenching by O<sub>2</sub>.** In solution, oxygen quenching of the excited state leads to an increase in the triplet yield.<sup>16</sup> However, for naphthalene on the alumina surface, no increase in the triplet absorbance was observed with 100% singlet quenching.<sup>16</sup> Since the oxygen singlet excited-state quenching mechanism for pyrene on SiO<sub>2</sub> has been shown to be temperature dependent, it is pertinent to inquire about the triplet excited-state quenching by oxygen on the SiO<sub>2</sub> surface. On the SiO<sub>2</sub> surfaces, at concentrations of added oxygen below 1 Torr at 298 K, the quantum yields of the pyrene and coronene triplet states increase. The maximum increase for the pyrene triplet is 20%, and is observed with the addition of about 1 Torr of oxygen (Figure 12). With additional oxygen, the triplet intensity decreases due to quenching of the triplet excited state. The singlet excited state is quenched by 40% with 1 Torr of added oxygen, and this quenching could give the triplet state. The sum of the quantum yields for pyrene by fluorescence (0.51) and triplet (0.22) is 0.73 for the sample in the absence of oxygen. In the presence of oxygen, additional triplet is obtained possibly via the mechanism given in eqs 8–11.

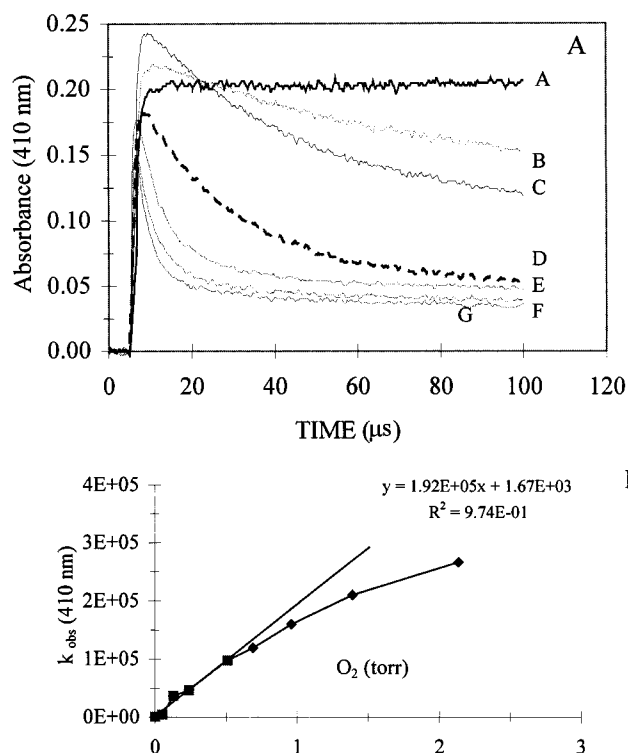


**Figure 12.** (A) Decay profiles of the pyrene triplet transient absorbance at 410 nm with added oxygen. Laser flash photolysis with 337 nm laser excitation of 0.5 μmol/g pyrene on 60 Å silica (*T<sub>a</sub>* = 150 °C) was observed with increasing oxygen pressures of 0 (A), 0.1 (B), 0.3 (C), 0.5 (D), 1.0 (E), 2.0 (F), and 4.5 torr (G). The constant baseline offset the traces D–G is from spectral overlap of the pyrene cation. (B) The observed decay rate calculated from the gaussian decay is plotted against the oxygen pressure. The calculated rate constants were determined from data collected with a 100 or 1000 μs collection window. The observed rate constant decreases to a near constant rate at high oxygen concentrations.



$$(Q_T) = 0.73 \left( \frac{k_2 + k_3(O_2)}{k_1 + k_2 + k_3(O_2)} \right) \quad (11)$$

The observed increase in the coronene triplet yield with added oxygen is even larger than that observed using pyrene. The coronene triplet quantum yield is 0.07 on porous silica gel which compares to 0.53 in ethanol and a literature value of 0.56 in ethanol.<sup>17</sup> The lifetime of the coronene triplet decreases with added oxygen on silica gel with a quenching rate constant of  $2.2 \times 10^9 \text{ L mol}^{-1} \text{ s}^{-1}$  at 298 K. At low concentrations of added oxygen (0–1 Torr), the intensity of the coronene triplet at 560 nm increases significantly. The increase being 50% with the addition of 0.5 Torr of oxygen. The singlet is quenched by 50% with the addition of 0.5 Torr oxygen, the oxygen concentration that shows the maximum triplet intensity increase. The fluorescence quantum yield is 0.22 without added oxygen. An increase in the triplet from 0.07 to 0.15 does not account for the 50% quenching of the singlet.

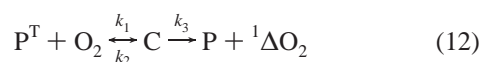
The pyrene triplet is quenched by oxygen on the 60 Å (*T<sub>a</sub>* = 150 °C) silica gel surface with a dynamic quenching rate constant of  $1.5 \times 10^5 \text{ Torr}^{-1} \text{ s}^{-1}$  ( $3 \times 10^9 \text{ L mol}^{-1} \text{ s}^{-1}$ ) at 298



K (Figure 12b). The same dynamic quenching rate constant is obtained for the 600 °C silica indicating the surface structure has a less significant effect on the triplet quenching rate than on the singlet excited-state rate. This compares to the singlet quenching rate constant of  $3.5 \times 10^6 \text{ Torr}^{-1} \text{ s}^{-1}$ .

Decreasing the sample temperature increases the concentration of oxygen adsorbed on the surface but does not increase the dynamic quenching rate constant. At 240 K, the dynamic quenching rate constant is  $3.3 \times 10^9 \text{ L mol}^{-1} \text{ s}^{-1}$  which is within 10% of the value at room temperature. This suggests that the triplet quenching mechanism results from collisional encounters on the surface. Decreasing the sample temperature does not change the dynamic quenching rate constant, and decreasing the sample temperature to 240 K shows a similar increase in the transient absorbance intensity with small additions of oxygen as is observed at 298 K. With oxygen concentrations above 1 Torr, the triplet intensity decreases more rapidly at 240 K than at room temperature. This results from the increased singlet quenching at decreased temperatures from adsorbed oxygen. The long triplet lifetime is selectively quenched by oxygen from vapor-phase collision encounter and not by adsorbed oxygen on the silica gel surface.

The rate of quenching of the pyrene triplet ( $P^T$ ) state decreases at oxygen pressures above 0.5 Torr. This is quite unlike the behavior of the singlet excited state, which is illustrated in Figure 3. A possible explanation for the above behavior is the formation of a complex C, between  $P^T$  and  $O_2$ ,



At low pressures the rate constant of process 3 is greater than that of process 1 or 2. Hence, the rate of the reaction approaches that of 1. At high pressures,  $k_1$ ,  $k_2$ , and  $k_3$  are comparable and the rate of the reaction is less than 1. Complex formation between the triplet and oxygen on the surface of  $SiO_2$  is suggested. The formation of complexes between excited states of aromatics and oxygen has been used to explain oxygen quenching previously.<sup>18</sup> A similar situation has been suggested for the gas-phase quenching of the triplet of benzene and oxygen.<sup>19</sup> Turro et. al.<sup>2a</sup> also note that the efficiency of  $O_2$  quenching of benzophenone triplet on  $SiO_2$  decreases with increasing  $O_2$  content. They report a change in mechanism to explain the data. The triplet quenching of benzophenone on increasing-pore-size silicas was described as resulting from a change from a Knudsen regime of quenching to a Langmuir–Hinshelwood mechanism. At this point it is not possible to pinpoint the actual mechanism of  $O_2$  quenching of triplet states of organic molecules adsorbed on  $SiO_2$ .

## Summary

The quenching of the singlet excited state of pyrene by  $O_2$  on several  $SiO_2$  silica surfaces occurs by two mechanisms, the LH and ER mechanisms. The relative contribution of each mechanism changes with the reaction temperature. The ER, or direct collision encounter, mechanism is dominant at high temperatures (>100 °C) and the surface diffusion, or LH,

mechanism is dominant at low temperatures (–80 °C). The efficiency of the reaction on the silica surface is lower than that in the gas phase. This is explained by simple geometric effects.

The results are supported by studies using NaCl. This surface approaches a flat surface and oxygen does not adsorb to the surface. In addition,  $O_2$  desorption studies demonstrate the adsorption of oxygen on the  $SiO_2$  surface and the increased residence times at lower temperatures.

The product of the singlet quenching reaction is the triplet state of pyrene. The yield of this reaction is lower than that in solution, unlike the singlets. The rate of quenching of the triplet state decreases with increasing oxygen pressure. It is suggested that this results from the formation of an intermediate complex on the surface.

**Acknowledgment.** The authors thank the National Science Foundation for support of this work. In addition, S. A. Ruetten thanks Bayer Corporation for support.

## References and Notes

- (1) (a) Rideal, E. K. *Proc. Cambridge Philos. Soc.* **1939**, 35, 130. (b) Hinshelwood, C. W. *Kinetics of Chemical Change*; Clarendon: Oxford, U.K., 1940.
- (2) (a) Drake, J. M.; Levitz, P.; Turro, N. J.; Nitsche, K. S.; Cassidy, K. F. *J. Phys. Chem.* **1988**, 92, 4680–4. (b) Levin, P. P.; Costa, S. M. B.; Vieira Ferreira, L. F.; Lopes, J. M.; Ribeiro, F. R. *J. Phys. Chem. B* **1997**, 101, 1355–1363.
- (3) (a) Krasnansky, R.; Koike, K.; Thomas, J. K. *J. Phys. Chem.* **1990**, 94, 4521. (b) Krasnansky, R.; Thomas, J. K. *J. Photochem. Photobiol. A: Chem.* **1991**, 57, 81–6. (c) Pankasem, S.; Thomas, J. K. *J. Phys. Chem.* **1991**, 95, 7385–93.
- (4) (a) Katz, O.; Samuel, J.; Avnir, D.; Ottolenghi, M. *J. Phys. Chem.* **1995**, 99, 14893–14902. (b) Wolfgang, S.; Gafney, H. D. *J. Phys. Chem.* **1983**, 87, 5395–5401.
- (5) (a) Iler, R. K. *The Chemistry of Silica*; John Wiley and Sons: New York, 1979. (b) Morrow, B. A. *Spectroscopic Characterization of Heterogeneous Catalysts: Studies in Surface Science and Catalysis*; Fierro, J. L. G., Ed.; Elsevier: Amsterdam, 1990; A161–A224.
- (6) (a) Marro, M.; Thomas, J. K. *J. Photochem. Photobiol. A: Chem.* **1993**, 57, 81–6. (b) Ruetten, S. A.; Thomas, J. K. *J. Phys. Chem. B* **1998**, 102, 598–606.
- (7) Wilkinson, F.; Beer, R. *Photochemical Processes in Organized Molecular Systems*; Honda, K., Ed.; Elsevier Science Publishers: New York, 1991; pp 377–396.
- (8) (a) Adamson, A. W. *Physical Chemistry of Surfaces*; John Wiley and Sons: New York, 1990. (b) Brunauer, S. *The Adsorption of Gases and Vapors*; Princeton University Press: London, 1943.
- (9) Aldrich Technical Data Sheet; W. R. Grace: Baltimore, MD, 1993.
- (10) Scherer, R.; Henglein, A. *Ber. Bunsen-ges. Phys. Chem.* **1977**, 81 (12), 1234–9.
- (11) Creary, X. *Org. Synth.* **1986**, 64, 207.
- (12) Silva, S.; Olea, A. F.; Thomas, J. K. *Photochem. Photobiol.* **1991**, 54 (4), 511–4.
- (13) (a) Jandris, L. J.; Force, R. K.; Yang, S. C. *Appl. Spectrosc.* **1985**, 39 (2), 266–8. (b) Haug, M.; Schulpin, H. *Appl. Spectrosc.* **1994**, 48 (4), 969–72.
- (14) Liu, X.; Thomas, J. K. *Langmuir* **1991**, 7, 2808–16.
- (15) Whitaker, T. J.; Bushaw, B. A. *J. Phys. Chem.* **1981**, 85, 2180–2.
- (16) (a) Richards, J. T.; West, G.; Thomas, J. K. *J. Phys. Chem.* **1970**, 74 (23), 4137–41. (b) Beck, G.; Thomas, J. K. *Chem. Phys. Lett.* **1983**, 94, 553–7.
- (17) Stevens, B.; Thomaz, M. F.; Jones, J. J. *Chem. Phys.* **1967**, 46, 405–6.
- (18) (a) Chihara, K.; Baba, H. *Chem. Phys.* **1977**, 25, 299. (b) Chihara, K.; Baba, H. *Bull. Chem. Soc. Jpn.* **1975**, 48, 3903.
- (19) Brown, R. G.; Phillips, D. *Chem. Phys.* **1973**, 630–636.